Fuel 357 (2024) 129905

Contents lists available at ScienceDirect

Fuel

journal homepage: www.elsevier.com/locate/fuel

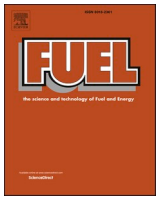

Full Length Article

Characterization of the quasi-liquid layer on gas hydrates with molecular dynamics simulations

Yifan Zhang, Senbo Xiao *, Rui Ma, Zhiliang Zhang *, Jianying He *

NTNU Nanomechanical Lab, Department of Structural Engineering, Norwegian University of Science and Technology (NTNU), Trondheim 7491, Norway

ARTICLE INFO

Keywords:
Hydrate stability
Quasi-liquid layer
QLL thickness
Instant displacement
Molecular dynamics

ABSTRACT

Understanding the properties of the surficial quasi-liquid layer (QLL) is a prerequisite in proper handling of gas hydrates, a potential alternative future energy resource. Despite of its critical importance, the characterization of QLL has long been known to be highly challenging. In this work, the evolution of QLL during hydrate decomposition was systematically investigated by Molecular Dynamics simulations. Using the instant displacement of water molecules as a measure of the fluidity of the molecular layer adjacent to hydrate surfaces, QLL thickness was accurately measured using the dynamic properties of water molecules for the first time. The QLL thickness obtained by this new molecular dynamics-based approach takes amorphous water molecules close to hydrate surfaces into account, which was often ignored in the previous results based on the static structural order parameters. The variation of QLL thickness throughout the hydrate decomposition process at different temperatures and pressures was then evaluated. The thickness of QLL was found to increase with elevated temperature and pressure, owing to the varied changes of the amorphous and hydrate-like molecular content in this important layer. The results regarding the dynamics of the QLL with molecular resolution improved the current understanding on the stability of gas hydrate and shed new light on the physical fundamentals relevant to future hydrate exploration as well as anti-hydrate materials design.

1. Introduction

Gas hydrate is a host–guest mixed cage-like solid substance formed by water and gas (methane, carbon monoxide, etc.) molecules under conditions of low temperature and high pressure [1]. Owing to its potential as an alternative energy storage medium, hydrate with cage structure has attracted great attention. Research on hydrates has been steadily progressing in many fields over the past few decades. There were a good number of studies focusing on the formation and dissociation processes [2–4] of hydrate for the understanding of specific micromechanisms observed in experiments, aiming for the further development of specific applications. Besides, hydrate formation and blockage of the pipeline system for the oil and gas exploitation in deep-sea water is still one of the biggest unsolved challenges in the energy production industry [5,6]. It is generally desired, via the investigation of their properties under varied ambient conditions, to understand gas hydrate behaviors in structural stability, surface adhesion, guest molecule content, and many others [7–11].

Understanding of the characteristics of hydrate surface is a prerequisite for almost all the research areas concerning hydrate. It is known that the surface of hydrate consists of an amorphous liquid-like water layer mixed with guest molecules, which is termed the Quasi-Liquid Layer (QLL) [12,13], as illustrated in Fig. 1. Similar to its known analogs on ice and other materials [14–19], the QLL of hydrate is also critically important to the properties of gas hydrates. Specifically, the presence of QLL has a direct impact on the decomposition of hydrates, namely the self-preservation phenomenon [20,21]. QLL can inhibit the further decomposition of internal hydrate due to its special quasi-liquid and viscous properties. QLL also plays an important role in hydrate growth by affecting the transport process of guest molecules for the formation of new cage structures. Furthermore, the structure and thickness of QLL are proven to have a significant effect on the adhesion of hydrate on solid surfaces [22,23]. The precise understanding of the thickness and structure of the QLL could also guide the field of hydrate phase changes on environmental issues and energy-related advances [24–26].

The thickness of QLL is extremely important for understanding its roles on the properties of hydrate. And it is currently known that the

* Corresponding authors.
E-mail addresses: senbo.xiao@ntnu.no (S. Xiao), zhiliang.zhang@ntnu.no (Z. Zhang), jianying.he@ntnu.no (J. He).

https://doi.org/10.1016/j.fuel.2023.129905
Received 15 June 2023; Received in revised form 31 August 2023; Accepted 20 September 2023
Available online 23 September 2023

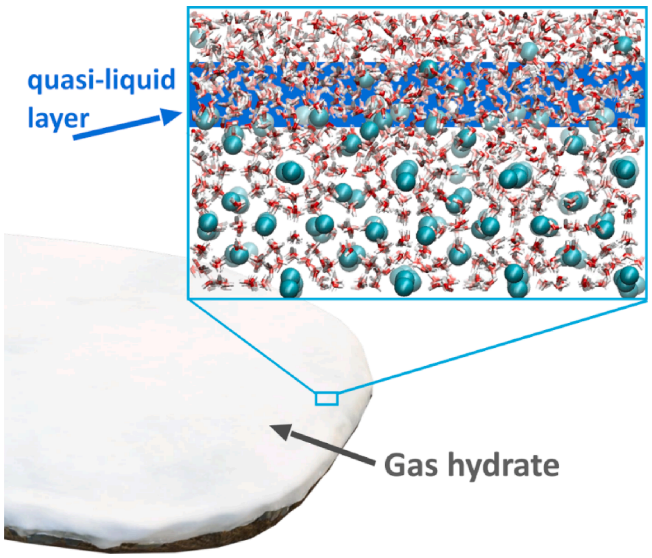

Fig. 1. Schematic illustration of the quasi-liquid layer on gas hydrate.

thickness of the QLL on the hydrate surface is in the range of a few nanometers [27–29]. Due to the small scale of QLL, there are many limitations in using experimental tools to detect the precise QLL thickness during QLL evolution. In comparison, Molecular dynamic (MD) simulation was proven to be a powerful tool for the investigation of the intriguing nanoscale events only observed in the QLL [27,30]. Using MD simulations, previous studies overwhelmingly focused on systems under temperature only below the hydrate melting point, and at the same time did not pay attention to the important responses of the QLL structure to the changes of system temperature and pressure. Furthermore, the previous simulation studies only mainly on the QLL at the hydrate-solid/vacuum interface, but not the hydrate/water interface that is more common in an actual pipeline. There is a good reason for the previous studies not to investigate QLL at the hydrate/water interface, as it is obviously difficult to distinguish the molecular structure of QLL from free water. In addition, the most common method for measuring QLL thickness in MD simulations is the F4 order parameter [31], which can identify the QLL through molecular structure differences among the water molecules. However, measuring the QLL only from the structural difference cannot give an accurate thickness due to the outermost unstructured and water-like region of the QLL [30]. Therefore, the dynamic definition and thickness analysis of QLL at the hydrate/water interface are not yet clear.

Herein, we performed MD simulations of the evolution of QLL during methane hydrate decomposition under different temperature and pressure conditions mimicking the pipeline internal environment. The aim of this study is (1) to accurately resolve QLL at the hydrate-water interface (2) to explore the evolution of QLL during the decomposition of hydrates above the melting point, and (3) to quantify the change of QLL thickness under different temperature and pressure conditions. The findings of this study focus on the mechanism of QLL evolution during hydrate decomposition at high temperatures and demonstrate the effect of environmental conditions on QLL thickness from a microscopic perspective.

2. Methodology

2.1. Model system and force-field parameters

A three-phase system consisting of gas (methane), water and hydrate was constructed for the simulation of the hydrate decomposition process, as shown in Fig. 2. The hydrate in the system contained $4 \times 4 \times 3$ *sI* hydrate unit cells, which consisted of 2944 water and 384 methane molecules. The hydrate structure was sandwiched by two water layers of 8000 water molecules, and further sandwiched by two gas layers of 1400 methane molecules in a simulation box with periodic boundary condition. The overall simulation box dimension of the configuration in the X-, Y-, and Z-direction was 26, 5, and 5 nm, respectively. This configuration of molecules in the simulation box reproduced the existence of multiple phases in a pipeline, which included hydrate/water interfaces featuring realistic conditions. The TIP4P-ICE model [32] was employed to describe the water molecules, while parameters from the OPLS-UA force field [33] were used for the methane molecules. The combination of the two molecular models was proven to produce credible results in previous studies [34–36].

2.2. Simulation settings

All the MD simulations were performed using Gromacs 2021.5 in this work [37]. The initial system was first energy minimized using the steepest descent method implemented in Gromacs, and further relaxed by a short equilibration of 2 ns under the NVT ensemble at a temperature of 300 K. The Newtonian equations of motion were integrated with the Velocity-Verlet algorithm [38] with a time step of 2 fs. In all the simulations, the non-bonded interactions were truncated at a cut-off distance of 1 nm, with the long-range electrostatics treated by the Particle Mesh Ewald method [39]. The system was then subjected to simulations under the NPT ensemble, with the hydrate decomposition conditions of temperature and pressure range of 280 to 320 K and 50–300 bar. It is worth noting that keeping the hydrate structure at the temperature range did not lead to sudden structural disintegration but gradual melting with the progression of the QLL layer into the hydrate structure. Due to the nanoscale size of the simulation systems, the temperature of the hydrate structure could be different from the bulk hydrate in melting experiments. The temperature was controlled by using the Nosé-Hoover algorithm [40] with a relaxation time of 0.4 ps. The pressure was

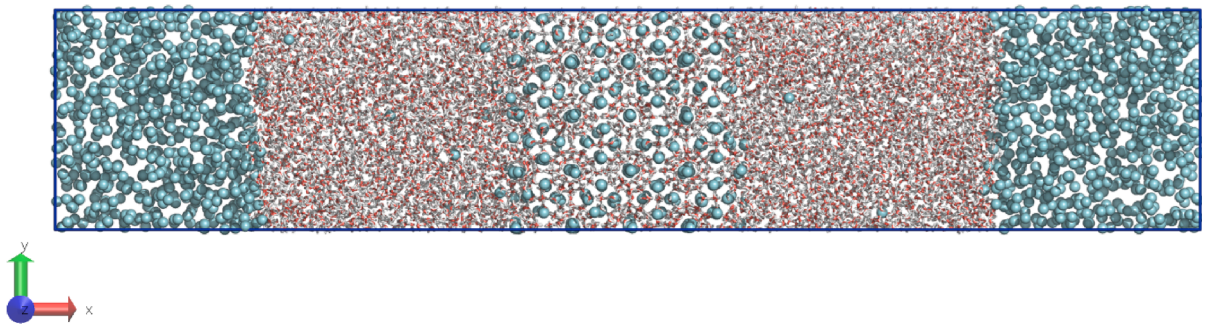

Fig. 2. Initial structure of the methane-water-hydrate three-phase system along the X-axis of the simulation box. The system contains 2944 water molecules (red and white spheres for oxygen and hydrogen respectively) and 384 methane molecules (cyan spheres) in the hydrate, 8000 water molecules in the water phase, and 1400 methane molecules (cyan sphere) in the gas phase. The same molecular color scheme was used in the other figures if not otherwise specified.

controlled using the Berendsen algorithm [41] with a relaxation time of 4 ps. Each simulation under specific temperature and pressure was carried out for 300 ns, with 5 parallel independent runs for the statistical reproducibility and reliability of the results.

2.3. QLL thickness measurement analysis method

The study of QLL thickness has always been an indispensable question of QLL-related research. Up to now, the thickness of QLL has been effectively measured by various methods in the experimental field [8,13]. However, due to the limitations of the QLL scale, the QLL thicknesses measured by different experimental methods are not uniform and do not give reliable results. Therefore, the thickness of QLL is tried to give a precise definition from the microscopic point of view. In the field of simulation, the most used method is the F4 order parameter. Because the F4 order parameter cannot take into account the outermost layer of amorphous water molecules (unstructured part) of the QLL, a novel method using the instant displacement of water molecules, that can consider the amorphous water layers, was used here for better quantification of the QLL. The thickness of QLL measured by the above two methods is compared in the results sections.

2.3.1. F4 order parameter

The F4 order parameter has been widely used to identify the structural arrangement of water molecule at the hydrate surface in MD simulations [42,43]. The F4 order measures the twist angle formed by the outermost hydrogen and oxygen of two adjacent water molecules away from the hydrate structure and has the definition as:

$$F4 = \frac{1}{n}\sum \cos 3Ø$$

where n is the total number of water-water pairs, Ø is the H–O …. O–H twist angle of the pair of two adjacent water molecules. The F4 order parameter is an average value obtained by averaging all water-water molecule pairs in the system, which reflects the different structure distributions within the system [43]. The corresponding values for the F4 order parameter are 0.7 and −0.04 for hydrate and bulk water, respectively.

The F4 order parameters of the whole model system in this work under 320 K and 100 bar is shown in Fig. 3 as an example. The F4 order parameter was measured every 0.1 nm along the x-axis to show the evolution more accurately. There is no value on both sides of the system because the F4 order parameter only measure the specific structure between the water molecules but not the gas molecules. As can be seen in Fig. 3(a), there are three regions of the F4 order parameter profile in the model system: the hydrate phase (around 0.7, the pink region in Fig. 3a), the water phase (around −0.04, yellow region), and the transition region (green region). And the transition region of the F4 order parameter profile can be considered as the QLL, continuously dropping from 0.7 to −0.04 (from ordered to amorphous). The F4 order parameters can be used to capture the changes of QLL in the system during hydrate decomposition, as shown in Fig. 3(b). At the beginning of the hydrate decomposition simulation, the QLL was located at the position close to the X-coordinate 10 nm and 14.5 nm of the simulation box (black curve, Fig. 3b). As the decomposition of hydrate progressed, the two transition regions of the F4 order parameter profile gradually migrated towards the hydrate at the center, signifying the shrinkage of the ordered hydrate structure. In the end, the F4 order parameter of the system was almost stable around −0.04 (brown curve, Fig. 3b), indicating the fully decomposition of hydrate structure in the model system. Using the F4 order parameter profile across the three phases in the system, the width of the transition region at the hydrate-water interface was taken as the thickness of QLL. In order to quantify the QLL thickness using the $D_{F4Parameter}$ profile, the so-called "10–90" criterion was applied in distinguishing the interfaces [44,45]. However, the "self-preservation" phenomenon [13] of hydrate suggests that the dynamic properties of water molecules in the QLL are significantly different from those in the hydrate and in the bulk water. As named by the "quasi-liquid" feature, water molecules at the outermost layer of QLL can be as amorphous as but dynamically different from bulk water. Example of similar water layers, termed "solvation layer", can be found on nanoparticles and biomolecules such as proteins in water [46,47]. This special water layer is part of QLL, which cannot be easily identified by a method relying on only analyzing the water structure such as the F4 order parameter. The thickness of QLL is urgently needed to be accurately measured by new methods.

2.3.2. Instant displacement

As such, a novel method is proposed to measure the thickness of the QLL through the molecular dynamic property, called the instant displacement ($D_{instant}$) of water molecules. Specifically, the displacement of each water molecule in the equilibrated model system was monitored

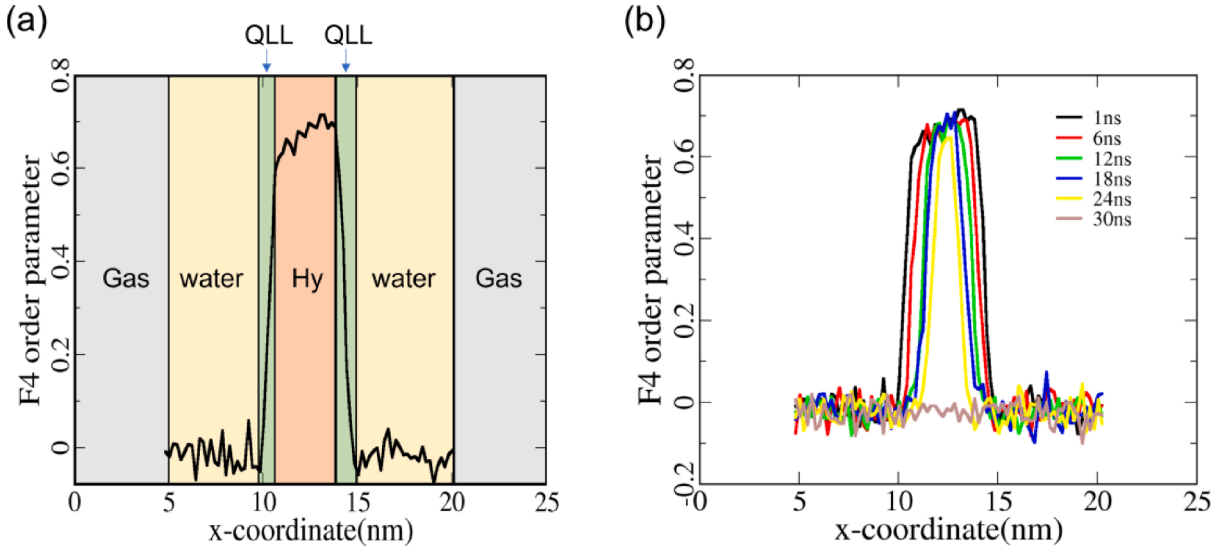

Fig. 3. F4 order parameter profile of the model system. (a) Three regions of the F4 order parameter profile representing the water (yellow), hydrate (pink) and QLL (green) along the X-direction of the simulation box. (b) The F4 order parameter profile at different simulation time of the model system under the temperature of 320 K and pressure of 100 bar.

for a sufficiently short simulation time window (Δt), as:

$$D_{instant} = \sqrt{(x_0 - x_{\Delta t})^2 + (y_0 - y_{\Delta t})^2 + (z_0 - z_{\Delta t})^2}$$

where x_0, y_0, z_0 are the initial x-, y- and z-coordinate of a water molecule, while $x_{\Delta t}$, $y_{\Delta t}$ and $z_{\Delta t}$ are the new coordinates of the same water molecule at the end of the time window Δt. By focusing on the dynamic properties of water molecules, the instant displacement can identify an accurate QLL with the previously missing "solvation layer", providing that the Δt was chosen correctly. Here in this work, Δt of 4,5,6 picoseconds were chosen to see if different Δt had any effect on QLL thickness (Suppl. Fig. S1). Since the results of 4,5 picoseconds were very similar, 5 ps was finally chosen for the clear distinguishing result after rounds of testing, as an example shown in Fig. 4. Specifically, the model system was first binned along the X-direction of the simulation box. $D_{instant}$ of all the water molecules in each binned layer of the model system was averaged and then normalized. Similar to F4 order parameter profiles, the $D_{instant}$ profile of the model system also exhibits three regions indicating bulk water (yellow region, Fig. 4), hydrate (pink region), and an obvious QLL at the hydrate-water interface (green region). The QLL identified by the $D_{instant}$ profile is obviously thicker than by the F4 order parameter profile above, showing the power of $D_{instant}$ in distinguishing the dynamic of the water molecules. In order to quantify the QLL thickness using the $D_{instant}$ profile, the so-called "10–90" criterion was applied in distinguishing the interfaces [44,45]. Specifically, the $D_{instant}$ profile was scanned along the X-axis of the simulation box. The x-coordinate with $D_{instant}$ value equal to 90 % of the average $D_{instant}$ in bulk water is taken as the beginning of the QLL, and 10 % higher than the average $D_{instant}$ in the hydrate as the end of the QLL. The "10–90" criterion can avoid data fluctuation to ensure the accuracy of measurement. Compared to the F4 order parameter, the new $D_{instant}$ approach considers the amorphous water molecules facing the bulk water, thus allowing an accurate description of the QLL region. It is worth noting that, compared with the more widely used mean square displacement (MSD) method, the instant displacement method is focusing on the short-time dynamic properties of water molecules, which is needed for the fast progressing of QLL during hydrate decomposition.

3. Results and discussion

3.1. QLL identified by two methods

Using $D_{instant}$ as a measure, the outermost amorphous water layer of QLL facing bulk water can indeed be resolved, resulting in higher thickness of QLL than using F4 order parameter. As the exemplifying result shown in Fig. 5, the QLL thickness on hydrate surface at a temperature of 320 K and pressure of 100 bar was found to be roughly 1.2 nm. As a comparison, the QLL thickness quantified by F4 order parameter is around 1.05 nm, which is similar to the result that has been observed in previous studies [48,49]. Indeed, most of the structures in the QLL obtained using F4 order parameter were cage-like or semi-cage-like structures with a few ring structures, missing the outermost molecular layer. $D_{instant}$ is thus a relatively more precise quantification for the identification of QLL, because the unstructured water solvation shell of hydrates is included. Given the QLL is highly important to the properties of hydrates, the outermost solvation layer of amorphous water molecules directly facing the surrounding environment of hydrates should always be accounted in the study of QLL. As such, it is recommended to use $D_{instant}$ for more accurate characterization of the QLL on hydrates.

Because the QLL is important to the decomposition rate of hydrate, precisely recognizing the QLL throughout the whole hydrate decomposition process is thus crucial. As a typical example of hydrate decomposition process observed in the modeling system shown in Fig. 6(a), the size of hydrate first steadily decreased, followed by an abrupt drop right before the hydrate completely disappeared. The decomposition of hydrate can also be illustrated by the radial distribution function (RDF) of water around methane molecules during simulation. Most obviously, the nearest peak of RDF of water molecules decreased with the simulation time, as shown in Suppl. Fig. S2. By monitoring the system snapshots during the decomposition process (Fig. 6b), the abrupt drop in the hydrate size occurred when the width of hydrate reached roughly one ring structure. It can be observed that the width of one cage structure is a critical size in the decomposition process, separating gradual steady melting and catastrophic disappearance. During steady melting, the thickness of QLL identified by F4 order parameter and $D_{instant}$ were roughly 1.05 and 1.2 nm, as shown in Fig. 6(c). QLL thickness measured using $D_{instant}$ is overall higher than that by F4 order parameter (red curve over black curve, Fig. 6c). As discussed above, $D_{instant}$ can recognize the outermost water layer belong to the QLL, which render thicker and more accurate QLL than F4 order parameter. Interestingly, QLL thickness by the two methods shown very different results after the melting hydrate reached the critical size of one ring structure. As indicated at the end of the profiles in Fig. 6(c), QLL thickness calculated by F4 order parameter also exhibited a sudden decrease when the hydrate was smaller than the critical size, featuring the abrupt drop of the hydrate size shown in Fig. 6

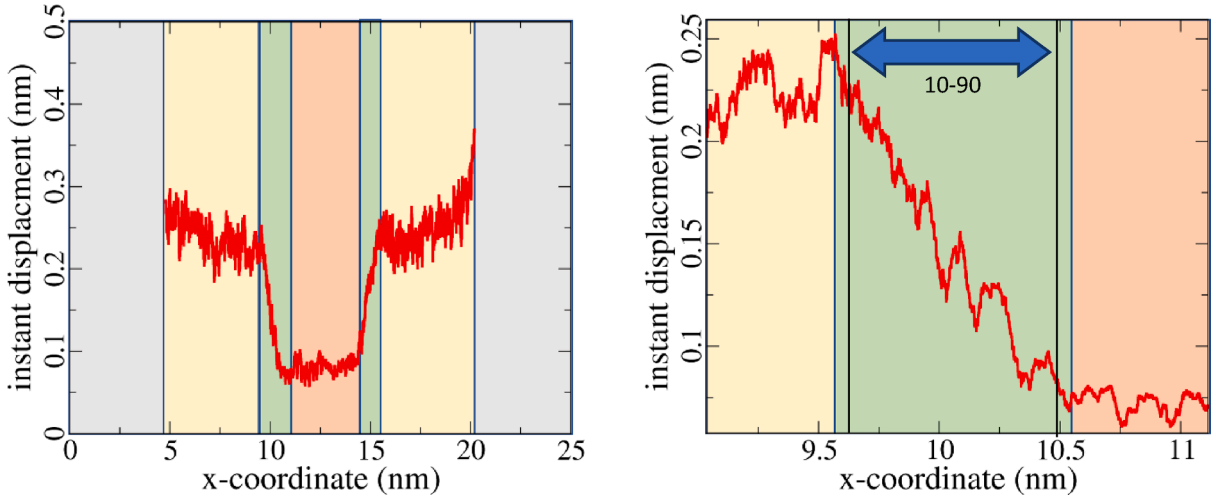

Fig. 4. Instant displacement ($D_{instant}$) of water molecules. (a) $D_{instant}$ profile in the model system at equilibrium under the temperature of 320 K and pressure of 100 bar. The grey, yellow, green and pink areas represent the methane, free water, QLL and hydrate respectively. $D_{instant}$ values are high close to the water–gas interface owing to high mobility in this area. (b) the "10–90" criterion used in quantifying the QLL region.

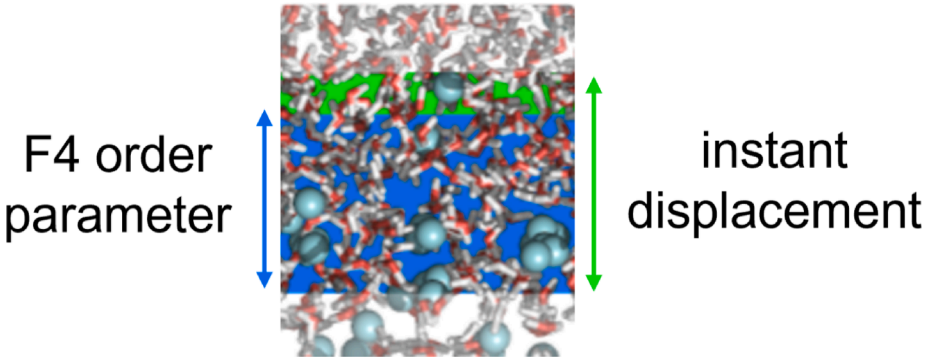

Fig. 5. Typical snapshots of QLL on the same hydrate surface are identified by the F4 order parameter (Blue region) and Instant Displacement (Blue and Green region). The top and bottom are free water and hydrate phase, respectively.

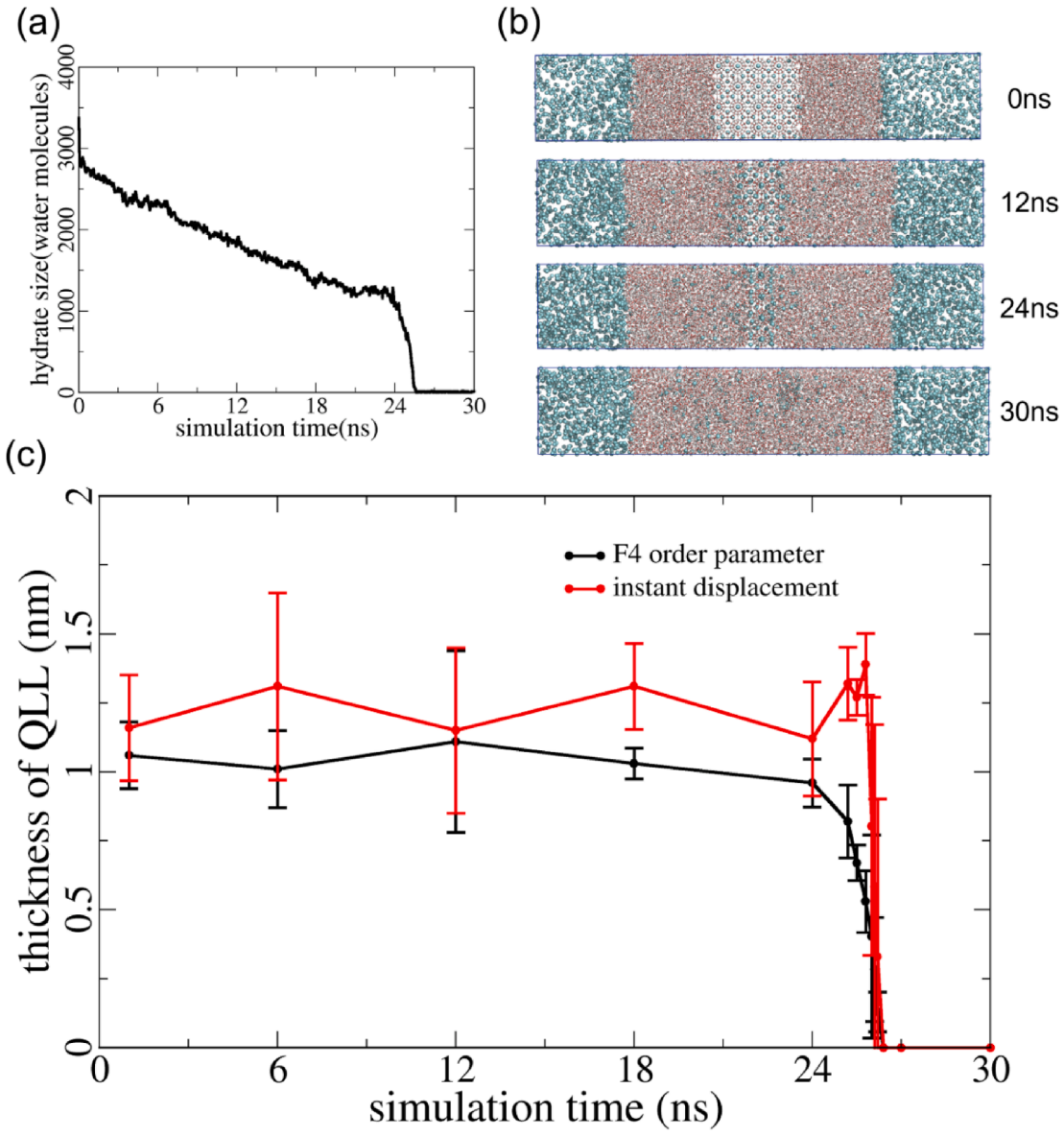

Fig. 6. The evolution of QLL during hydrate decomposition. (a) a typical hydrate size change profile under a temperature of 320 K and a pressure of 100 bar. The number of water molecules in hydrate structure is taken as the size of hydrate [52]. (b) The snapshots of the decomposition process shown in (a). (c) QLL thickness recognized by F4 order parameter and by $D_{instant}$.

(a). In contrast, QLL thickness calculated by $D_{instant}$ shown an extra obvious increase before the final sudden decrease (red curve, Fig. 6c). The increase in the QLL increase recognized by $D_{instant}$ was further confirmed by independent simulations at a higher temperature of 310 K, as result shown in Suppl. Fig. S3. Because the instant displacement quantifies the dynamic properties of the water molecules, the result thus indicated an increase in the mobility of the water molecules of the remaining hydrate structure right before the fully decomposition event (sudden drop in hydrate size, Fig. 6a). Indeed, the instance displacement level of remaining hydrate structure increased obviously right before fully decomposition, as shown in Suppl. Fig. S4. The difference of QLL thickness obtained by the two methods also indicates a delay in time in the hydrate decomposition, during which the water molecules in the hydrate of critical size swiftly lost the hydrate structure, maintained a mixed state with guest molecules, and then gained the dynamic properties as bulk water. This time difference is roughly 1 ns in the example shown in Fig. 6(c) (from 25 to 26 ns, red curve). The result raised an interesting question concerning the so-called secondary formation of hydrate in experiments, namely hydrate can form again in a short time in mixed systems right after hydrate melting [50,51]. The delay in time observed here for newly melted water molecules from hydrate structure to become bulk water seems to favor the hypothesis of good mixed state for hydrate secondary formation.

3.2. QLL at different temperatures

The QLL was believed to have a so-called self-preservation effect impacting hydrate dissociation rate [17]. Temperature-dependent QLL-related properties such as structure and thickness can have a significant impact on self-preservation capabilities. It is thus interesting to gain an in-depth view of the QLL during hydrate steady decomposition under varied temperatures. To do so, the model system was subjected to a pressure of 100 bar in a temperature range of 280 to 320 K. The steady decomposition of hydrate can be identified by the hydrate size as shown in Fig. 6(a), and by the potential energy. Specifically, the steady decomposition of hydrate structures leads to the loss of stable hydrogen bonds in the system, which further results in the gradual increase of the potential energy. As the potential energy at the chosen temperature shown in Suppl. Fig. S5, there is no observable hydrate decomposition at 280 K. At other temperatures, the hydrate decomposition is obvious, with the higher temperature the higher the decomposition rate. The QLL indeed showed clear response to the change of temperature.

Most strikingly, the structure of QLL was different at different temperatures. As snapshots shown in Suppl. Fig. S6(a), the QLL region in all the simulations included an amorphous and a hydrate-like region as the detailed identified method provided in the Supplementary Materials (Suppl. Fig. S7). At a low temperature of 280 K, the QLL mainly consisted of a hydrate-like region. With the increase of temperature, the QLL contained a gradually increasing content of amorphous region (Suppl. Fig. S6(b)). Furthermore, the QLL also contained an increasing methane concentration in the amorphous region as the temperature increased, which could be resulted from the elevated rate of hydrate decomposition and not sufficient time for the diffusion of the methane molecules. The increase in the amorphous region in the QLL resulted in thicker QLL, as depicted in Fig. 7(b). Overall, the thickness of QLL showed a significant increase with the increase of the system temperature, which agreed with observations in previous studies on the self-protection phenomenon of hydrates [53]. Here, the thickening of the amorphous region at higher temperatures and the accumulated high concentration of guest molecules was also in line with the self-preservation effect. Besides, the QLL thickness measured by instant displacement is larger than that measured by the F4 order parameter at all temperatures as comparison shown in Suppl. Fig. S8, which further confirmed the result in Fig. 6(c).

3.3. QLL under different pressure

It was confirmed by experiments that the decomposition rate of hydrate gradually decreases with the increase of pressure [54]. The decomposition rate of hydrate monitored in the simulation also followed the same trend, namely the higher pressure the slower decomposition. The model system was subjected to a temperature of 290 K in a pressure range of 50 to 300 bar. As shown by Suppl. Fig. S9, the system potential energy profile shows the highest increase slope under the lowest pressure of 50 bar, the fastest breaking down of hydrogen bonds and thus the hydrate structure. It is worth noting the hydrate structure not only was stable but also grew slightly under a pressure of 300 bar during the whole simulation, as demonstrated by the system snapshots shown in Suppl. Fig. S10, leading to no significant potential energy changes in the system.

The QLL also responds to the change of pressure in the system. Under low pressure, the QLL is mainly dominated by the hydrate-like structure as shown in Fig. 8a. With the increased pressure, the QLL also includes

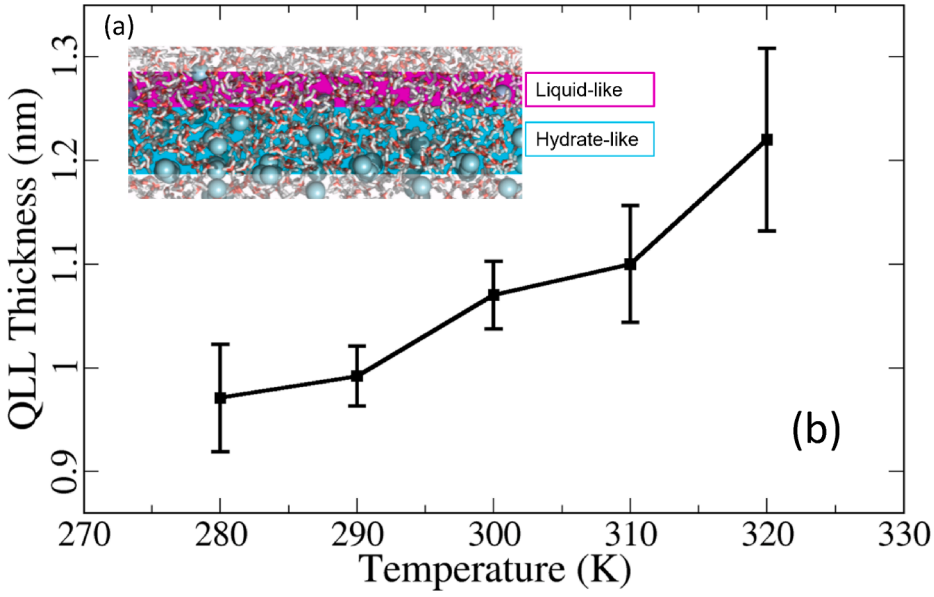

Fig. 7. QLL at different temperatures. (a) QLL captured during the steady decomposition of hydrate. The amorphous and structured regions in the QLL are indicated by pink and blue, respectively. (b) QLL thickness at different temperatures. The error bars show standard deviation of 5 independent simulations.

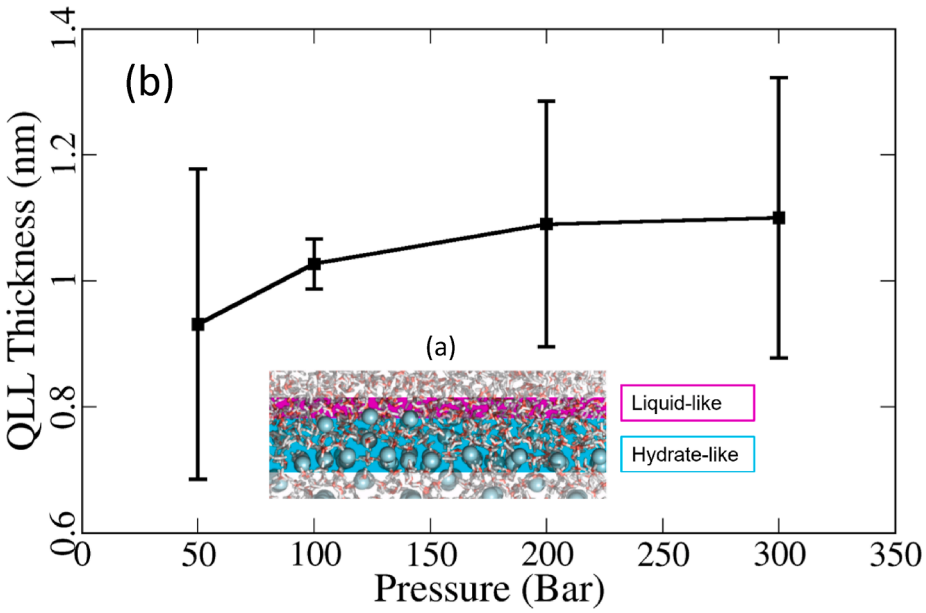

Fig. 8. QLL under different pressure. (a) QLL captured during the steady decomposition of hydrate. The amorphous and structured regions in the QLL are indicated by pink and blue, respectively. (b) QLL thickness measured under different pressure. The error bars show the standard deviation of 5 independent simulations.

an increasing content of amorphous structure (Suppl. Fig. S11(b)). Accordingly, the QLL slightly thickened with increasing pressure, from 0.93 nm under 50 bar to 1.10 nm under 300 bar as shown in Fig. 8(b). Specifically, the QLL thickness increased significantly from 50 bar to 200 bar, but less obviously from 200 to 300 bar. The increase of QLL thickness with high pressure was also confirmed by measurement using the F4 order parameter, as shown in Suppl. Fig. S12, and at different temperatures (Suppl. Fig. S13). It is interesting to note that the thickening QLL and the decreased hydrate decomposition coincided with the increase of pressure. This result again suggested that the thickness of the QLL play important roles in hydrate decomposition rate, which might also be explained by the self-preservation effect by the previous study [20,21].

4. Conclusion

In this work, the decomposition of methane hydrate under different temperature and pressure conditions was investigated by using molecular dynamics simulations with focusing on the changes in the structure and thickness of the QLL. A new characterization approach of the QLL based on the instant displacement of water molecules was proposed, which uses the dynamics properties of water molecules instead of the structural properties for taking into account the amorphous regions of QLL. The QLL was found to maintain a stable thickness during the steady decomposition of hydrate but showed a previously unresolved increase right before the complete disappearance of hydrate. Overall, the QLL thickness was found to increase with elevated temperature and pressure, which was attributed to the different molecular content in the QLL. There was an increasing content of amorphous water molecules in the QLL with the increased temperature and pressure. Specifically, high temperature increased hydrate decomposition rate, which resulted in thickening of the QLL with viscous amorphous water and increased gas content. Higher pressure also resulted in larger thickness of the QLL, which is associated with stable hydrate and hindered decomposition. The thickness of the QLL seemed to play an important role in the hydrate decomposition process. It is a challenging and interesting topic for future studies to assess the thermal conductivity and interface pressure of the thickening QLL for a better understanding of its function in hydrate decomposition. Besides, the influence of methane concentration in the QLL is not considered in this work due to the fast migration dynamics of the released methane. However, the concentration of methane in the water phase could influence the QLL properties or thickness, which should be taken into account in experiments. The results detailed the evolution of the molecule composition in the QLL throughout the hydrate decomposition process at varied conditions, which provided new reference for the understanding of hydrates and their interaction with the environment, shedding light on the theoretical basis of unexplained phenomena of hydrate such as self-preservation, secondary formation and so on in experiment and applications.

CRediT authorship contribution statement

Yifan Zhang: Writing – review & editing, Writing – original draft, Visualization, Validation, Software, Methodology, Investigation, Formal analysis, Data curation, Conceptualization. **Senbo Xiao:** Writing – review & editing, Validation, Supervision, Software, Methodology, Formal analysis, Conceptualization. **Rui Ma:** Software, Methodology, Investigation. **Zhiliang Zhang:** Writing – review & editing, Validation, Supervision, Funding acquisition, Conceptualization. **Jianying He:** Writing – review & editing, Validation, Supervision, Conceptualization.

Declaration of Competing Interest

The authors declare that they have no known competing financial interests or personal relationships that could have appeared to influence the work reported in this paper.

Data availability

Data will be made available on request.

Acknowledgments

We are grateful for the support of the Research Council of Norway through the D'andra project (Grant No. 302348) and the Chinese Scholarship Council. The supercomputer CPU hours were provided by the Norwegian Metacenter for Computational Science (Grant No. NN9110K, NN9391K, and NN8084K).

Appendix A. Supplementary material

Supplementary data to this article can be found online at https://doi.org/10.1016/j.fuel.2023.129905.

References

[1] Sloan Jr ED, Koh CA. Clathrate hydrates of natural gases. CRC Press; 2007.
[2] English NJ, Lauricella M, Meloni S. Massively parallel molecular dynamics simulation of formation of clathrate-hydrate precursors at planar water-methane interfaces: Insights into heterogeneous nucleation. J Chem Phys 2014;140(20):204714. https://doi.org/10.1063/1.4879777.
[3] Zhong JR, Sun YF, Li WZ, et al. Structural transition range of methane-ethane gas hydrates during decomposition below ice point. Appl Energy 2019;250:873–81. https://doi.org/10.1016/j.apenergy.2019.05.092.
[4] Linga P, Clarke MA. A review of reactor designs and materials employed for increasing the rate of gas hydrate formation. Energy Fuel 2017;31(1):1–13. https://doi.org/10.1021/acs.energyfuels.6b02304.
[5] Akhfash M, Aman ZM, Ahn SY, et al. Gas hydrate plug formation in partially-dispersed water–oil systems. Chem Eng Sci 2016;140:337–47. https://doi.org/10.1016/j.ces.2015.09.032.
[6] Huo Z, Freer E, Lamar M, et al. Hydrate plug prevention by anti-agglomeration. Chem Eng Sci 2001;56(17):4979–91. https://doi.org/10.1016/S0009-2509(01)00188-9.
[7] Liu C, Li M, Chen L, et al. Experimental investigation on the interaction forces between clathrate hydrate particles in the presence of a water bridge. Energy Fuel 2017;31(5):4981–8. https://doi.org/10.1021/acs.energyfuels.7b00364.
[8] Nguyen NN, Berger R, Kappl M, et al. Clathrate adhesion induced by Quasi-liquid layer. J Phys Chem C 2021;125(38):21293–300. https://doi.org/10.1021/acs.jpcc.1c06997.
[9] Ma R, Wang F, Chang Y, et al. Unraveling adhesion strength between gas hydrate and solid surfaces. Langmuir 2021;37(47):13873–81. https://doi.org/10.1021/acs.langmuir.1c02315.
[10] Gupta A, Baron GV, Perreault P, et al. Hydrogen clathrates: Next generation hydrogen storage materials. Energy Storage Mater 2021;41:69–107. https://doi.org/10.1016/j.ensm.2021.05.044.
[11] Surovtseva D, Amin R, Barifcani A. Design and operation of pilot plant for CO_2 capture from IGCC flue gases by combined cryogenic and hydrate method. Chem Eng Res Des 2011;89(9):1752–7. https://doi.org/10.1016/j.cherd.2010.08.016.
[12] Maeda N, Maeda N. Nucleation of gas hydrates. Springer International Publishing; 2020.
[13] Nguyen NN, Berger R, Butt HJ. Surface premelting and interfacial interactions of semi-clathrate hydrate. J Phys Chem C 2019;123(39):24080–6. https://doi.org/10.1021/acs.jpcc.9b06376.
[14] Luo J. Stabilization of nanoscale quasi-liquid interfacial films in inorganic materials: a review and critical assessment. Crit Rev Solid State Mater Sci 2007;32(1–2):67–109. https://doi.org/10.1080/10408430701364388.
[15] Davies PL. Ice-binding proteins: a remarkable diversity of structures for stopping and starting ice growth. Trends Biochem Sci 2014;39(11):548–55. https://doi.org/10.1016/j.tibs.2014.09.005.
[16] Faraday M. Experimental researches in chemistry and physics. CRC Press; 1990.
[17] Bartels-Rausch T, Jacobi HW, Kahan TF, et al. A review of air–ice chemical and physical interactions (AICI): liquids, quasi-liquids, and solids in snow. Atmos Chem Phys 2014;14(3):1587–633. https://doi.org/10.5194/acp-14-1587-2014.
[18] Kahan TF, Reid JP, Donaldson DJ. Spectroscopic probes of the quasi-liquid layer on ice. Chem A Eur J 2007;111(43):11006–12. https://doi.org/10.1021/jp074551o.
[19] Slater B, Michaelides A. Surface premelting of water ice. Nat Rev Chem 2019;3(3):172–88. https://doi.org/10.1038/s41570-019-0080-8.
[20] Takeya S, Ebinuma T, Uchida T, et al. Self-preservation effect and dissociation rates of CH4 hydrate. J Cryst Growth 2002;237:379–82. https://doi.org/10.1016/S0022-0248(01)01946-7.
[21] Li B, Zhang TT, Wan QC, et al. Kinetic study of methane hydrate development involving the role of self-preservation effect in frozen sandy sediments. Appl Energy 2021;300:117398. https://doi.org/10.1016/j.apenergy.2021.117398.
[22] Nguyen NN, Berger R, Kappl M, et al. Clathrate adhesion induced by Quasi-liquid layer. J Phys Chem C 2021;125(38):21293–300. https://doi.org/10.1021/acs.jpcc.1c06997.
[23] Ma R, Xiao S, Chang Y, et al. An interfacial gas-enrichment strategy for mitigating hydrate adhesion and blockage. Chem Eng J 2023;453:139918. https://doi.org/10.1016/j.cej.2022.139918.
[24] Sun L, et al. "A hydrate-based zero liquid discharge method for high-concentration organic wastewater: resource recovery and water reclamation. NPJ Clean Water 2023;6(1):49. https://doi.org/10.1038/s41545-023-00262-w.
[25] Hyunho K, Junjie Z, Zhenyuan Y, et al. An electrical resistivity-based method for measuring semi-clathrate hydrate formation kinetics: Application for cold storage and transport. Appl Energy 2022;308:118397. https://doi.org/10.1016/j.apenergy.2021.118397.
[26] Ponnivalavan B, Abhishek N, et al. A review of clathrate hydrate based desalination to strengthen energy-water nexus. ACS Sustain Chem Eng 2018;6(7):8093–107. https://doi.org/10.1021/acssuschemeng.8b01616.
[27] Ding LY, Geng CY, Zhao YH, et al. Molecular dynamics simulation for surface melting and self-preservation effect of methane hydrate. Sci China, Ser B 2008;51:651–60. https://doi.org/10.1007/s11426-008-0016-5.
[28] English NJ, MacElroy JMD. Perspectives on molecular simulation of clathrate hydrates: Progress, prospects and challenges. Chem Eng Sci 2015;121:133–56. https://doi.org/10.1016/j.ces.2014.07.047.
[29] Gao F, Gupta KM, Yuan S, et al. Decomposition of CH4 hydrate: effects of temperature and salt from molecular simulations. Mol Simul 2018;44(15):1220–8. https://doi.org/10.1080/08927022.2018.1478090.
[30] Shepherd TD, Koc MA, Molinero V. The quasi-liquid layer of ice under conditions of methane clathrate formation. J Phys Chem C 2012;116(22):12172–80. https://doi.org/10.1021/jp303605t.
[31] Zhang Z, Guo GJ. The effects of ice on methane hydrate nucleation: a microcanonical molecular dynamics study. PCCP 2017;19(29):19496–505. https://doi.org/10.1039/C7CP03649C.
[32] Abascal JLF, Sanz E, García Fernández R, et al. A potential model for the study of ices and amorphous water: TIP4P/Ice. J Chem Phys 2005;122(23):234511. https://doi.org/10.1063/1.1931662.
[33] Jorgensen WL, Madura JD, Swenson CJ. Optimized intermolecular potential functions for liquid hydrocarbons. J Am Chem Soc 1984;106(22):6638–46. https://doi.org/10.1021/ja00334a030.
[34] Sanchez-Burgos Ignacio, et al. Homogeneous ice nucleation rates for mW and TIP4P/ICE models through Lattice Mold calculations. The Journal of Chemical Physics 2022;157(9). https://doi.org/10.1063/5.0101383.
[35] Linse JB, Hub JS. Three-and four-site models for heavy water: SPC/E-HW, TIP3P-HW, and TIP4P/2005-HW. J Chem Phys 2021;154(19):194501. https://doi.org/10.1063/5.0050841.
[36] Martin MG. Comparison of the AMBER, CHARMM, COMPASS, GROMOS, OPLS, TraPPE and UFF force fields for prediction of vapor–liquid coexistence curves and liquid densities. Fluid Phase Equilib 2006;248(1):50–5. https://doi.org/10.1016/j.fluid.2006.07.014.
[37] Van Der Spoel D, Lindahl E, Hess B, et al. GROMACS: fast, flexible, and free. J Comput Chem 2005;26(16):1701–18. https://doi.org/10.1002/jcc.20291.
[38] Molinero V, Moore EB. Water modeled as an intermediate element between carbon and silicon. J Phys Chem B 2009;113(13):4008–16. https://doi.org/10.1021/jp805227c.
[39] York DM, Darden TA, Pedersen LG. The effect of long-range electrostatic interactions in simulations of macromolecular crystals: A comparison of the Ewald and truncated list methods. J Chem Phys 1993;99(10):8345–8. https://doi.org/10.1063/1.465608.
[40] Hoover WG. Constant-pressure equations of motion. Phys Rev A 1986;34(3):2499. https://doi.org/10.1103/PhysRevA.34.2499.
[41] Berendsen HJC, Postma JPM, Van Gunsteren WF, et al. Molecular dynamics with coupling to an external bath. J Chem Phys 1984;81(8):3684–90. https://doi.org/10.1063/1.448118.
[42] Walsh MR, Koh CA, Sloan ED, et al. Microsecond simulations of spontaneous methane hydrate nucleation and growth. Science 2009;326(5956):1095–8. https://doi.org/10.1126/science.1174010.
[43] Choudhary N, Das S, Roy S, et al. Effect of polyvinylpyrrolidone at methane hydrate-liquid water interface. Application in flow assurance and natural gas hydrate exploitation. Fuel 2016;186:613–22. https://doi.org/10.1016/j.fuel.2016.09.004.
[44] Chang Y, Xiao S, Fu Y, et al. Nanomechanical characteristics of trapped oil droplets with nanoparticles: a molecular dynamics simulation. J Pet Sci Eng 2021;203:108649. https://doi.org/10.1016/j.petrol.2021.108649.
[45] Rivera JL, McCabe C, Cummings PT. Molecular simulations of liquid-liquid interfacial properties: Water–n-alkane and water-methanol–n-alkane systems. Phys Rev E 2003;67(1):011603. https://doi.org/10.1103/PhysRevE.67.011603.
[46] Song S, Peng C. Thickness of solvation layers on nano-scale silica dispersed in water and ethanol. J Dispers Sci Technol 2005;26(2):197–201. https://doi.org/10.1081/DIS-200045588.
[47] Dahanayake JN, Mitchell-Koch KR. How does solvation layer mobility affect protein structural dynamics? Front Mol Biosci 2018;5:65. https://doi.org/10.3389/fmolb.2018.00065.
[48] Bagherzadeh SA, Alavi S, Ripmeester JA, et al. Evolution of methane during gas hydrate dissociation. Fluid Phase Equilib 2013;358:114–20. https://doi.org/10.1016/j.fluid.2013.08.017.
[49] Bagherzadeh SA, Englezos P, Alavi S, et al. Molecular modeling of the dissociation of methane hydrate in contact with a silica surface. J Phys Chem B 2012;116(10):3188–97. https://doi.org/10.1021/jp2086544.
[50] Kou X, Feng JC, Li XS, et al. Memory effect of gas hydrate: Influencing factors of hydrate reformation and dissociation behaviors. Appl Energy 2022;306:118015. https://doi.org/10.1016/j.apenergy.2021.118015.
[51] Gambelli AM. Variations in terms of CO2 capture and CH4 recovery during replacement processes in gas hydrate reservoirs, associated to the "memory effect". J Clean Prod 2022;360:132154. https://doi.org/10.1016/j.jclepro.2022.132154.
[52] Li L, Zhong J, Yan Y, et al. Unraveling nucleation pathway in methane clathrate formation. Proc Nat Acad Sci 2020;117(40):24701–8. https://doi.org/10.1073/pnas.2011755117.
[53] Jiménez-Ángeles F, Firoozabadi A. Induced charge density and thin liquid film at hydrate/methane gas interfaces. J Phys Chem C 2014;118(45):26041–8. https://doi.org/10.1021/jp507160s.
[54] Sun W, Wei N, Zhao J, et al. Imitating possible consequences of drilling through marine hydrate reservoir. Energy 2022;239:121802. https://doi.org/10.1016/j.energy.2021.121802.